Electrochemistry Communications 39 (2014) 26–29

Contents lists available at ScienceDirect

Electrochemistry Communications

journal homepage: www.elsevier.com/locate/elecom

Short communication

Multi-walled carbon nanotubes/graphene nanoribbons hybrid materials with superior electrochemical performance

Javier Hernández-Ferrer [a,*], Pablo Laporta [a], Fabiana Gutiérrez [b], María D. Rubianes [b], Gustavo Rivas [b], Mª Teresa Martínez [a]

[a] Instituto de Carboquímica (CSIC), C/Miguel Luesma Castán 4, E-50018 Zaragoza, Spain
[b] Instituto de Investigaciones en Físico Química de Córdoba (INFIQC) CONICET-UNC, Departamento de Físico Química, Facultad de Ciencias Químicas, Universidad Nacional de Córdoba, Ciudad Universitaria, 5000 Córdoba, Argentina

ARTICLE INFO

Article history:
Received 31 October 2013
Received in revised form 3 December 2013
Accepted 6 December 2013
Available online 14 December 2013

Keywords:
Graphene nanoribbons
Hybrid materials
Electrochemical sensing

ABSTRACT

Graphene nanoribbons (GNRs) were synthesized by oxidation of arc discharge multi-walled carbon nanotubes (MWCNTs) in concentrated H_2SO_4 using $KMnO_4$ as oxidizing agent at different times from 15 to 120 min. One of the GNR samples was further electrochemically and chemically reduced. The material obtained after 15 min of oxidation time (GNR_{015}) was a hybrid material containing MWCNTs, partially unzipped GNRs-MWCNTs and fully unzipped GNRs, and it demonstrated a superior electrochemical performance. This material presented the highest heterogeneous charge transfer constant and sensitivity towards H_2O_2 reduction. These properties are due to the balance between the content of unzipped MWCNTs, C_{sp2} carbon structure and oxygen moieties. GNR_{015}, thus reveals as a promising platform for further applications in electrochemical sensing.

1. Introduction

Graphene is a hot topic in materials science. In the last years, several papers have been focused on the preparation and applications of graphene nanoribbons (GNRs) using Tour's method, consisting in the longitudinal unzipping of multi-walled carbon nanotubes (MWCNTs) [1,2]. Electrochemistry of graphene (in all its forms) [3] and CNTs [4] has been widely studied. Metal content [5], available electrochemical area [6], oxygen moieties/edge chemistry [7], and functionalization [8] have demonstrated to have a great influence on the electrochemical properties of carbon nanomaterials, and all of them must be considered to gain a fruitful insight.

Graphene-CNT hybrids have been revealed as promising materials in electrochemical applications [9,10]. Synergic effects between both materials have been reported [10], although this synergy, is not observed by other authors [11]. The preparation of graphene-CNT hybrids is usually performed using a high-cost and time-consuming method involving several steps, i.e. graphene oxide synthesis, reduction, and mixing of graphene oxide, reduced graphene oxide and CNTs to obtain material's best performance [10]. Another approach to obtain the graphene-CNT hybrid material is using MWCNTs as carbon source. The procedure starts with MWCNTs and ends in GNRs, having in the middle several GNR-MWCNT hybrid materials with different characteristics. Controlling the reaction conditions [9], a material with optimal electrochemical properties should be obtained.

The objective of the work is to synthesize electroactive MWCNT-based nanomaterials for the development of efficient electrochemical (bio)sensors. The significance of the work is that we have determined with an exhaustive structural and electrochemical characterization, that a hybrid nanomaterial with low oxidation degree and having an optimal balance of conductive C_{sp2} and electroactive oxygen groups, presents an excellent electrochemical performance. This nanomaterial was prepared by a low-cost and simple methodology.

2. Experimental

2.1. Material synthesis

GNRs were synthesized using Tour's method [1,2]. Briefly, 150 mg of arc-discharge MWCNTs [12] were dispersed by ultrasonication in 150 mL of concentrated H_2SO_4. Afterwards, the dispersion was heated up to 65 ºC and 750 mg of $KMnO_4$ were added. The different materials were prepared by heating the dispersion for 15 (GNR_{015}), 30 (GNR_{030}), 60 (GNR_{060}), 90 (GNR_{090}), 100 (GNR_{100}) and 120 (GNR_{120}) min.

A portion of GNR_{120} was reduced using N_2H_4 ($GNR_{120\text{-}N2H4}$), following a protocol previously described [2].

2.2. Electrode preparation

The materials were dispersed in 1.0% of NH_4OH solution to obtain a dispersion of 1.0 mg/mL. The GCE was polished with alumina slurries of 0.30 and 0.05 μm. Afterwards, they were modified by drop coating with 10 μL of the dispersions, evaporating the solvent at room temperature.

* Corresponding author. Tel.: +34 976 733977; fax: +34 976 733318.
E-mail address: jhernandez@icb.csic.es (J. Hernández-Ferrer).

1388-2481/$ – see front matter © 2013 Elsevier B.V. All rights reserved.
http://dx.doi.org/10.1016/j.elecom.2013.12.006

GCEs modified with untreated MWCNTs (GNR_{000}) were also used as control.

2.3. Apparatus

X-ray diffraction (XRD) was done with a Bruker D8 Advance Series 2 instrument, Transmission Electron Microscopy (TEM) images were obtained with a INCA 200 X-Sight, (Oxford Instruments) microscope. X-ray photoelectron spectroscopy (XPS) was carried out on a ESCAPlus Omicron. Direct oxygen determinations were carried out with a Thermo Flash 1112 analyzer. Electrochemical experiments were performed with Epsilon (BAS), Autolab 128N and TEQ-04 potentiostats. Scanning Electronic Microscopy (FE-SEM) images were obtained with a Field Emission Gun Scanning Electron Microscopy (FE-SEM Zeiss, ΣIGMA model). BET area was determined with a Micromeritics ASAP 2020 analyzer, using N_2 adsorption isotherm at 77 K, with degasification at 150 ºC for 300 min.

2.4. Electrochemical procedure

A 0.010 M phosphate buffer solution pH 7.40 containing 0.100 M NaCl was the supporting electrolyte. A platinum wire and Ag/AgCl, 3 M KCl were used as counter and reference electrodes, respectively.

Amperometry was carried out by applying the desired potential and allowing the transient current to reach steady-state prior to the addition of the analyte. Heterogeneous electron transfer rate constants (k_0) were calculated according to the Nicholson method [13] from cyclic voltammograms of 2.0×10^{-3} M $K_3Fe(CN)_6$ performed by scanning the potential between −0.200 and 0.400 V. Electroactive areas were calculated by chronocoulometry [14] using 1.0×10^{-3} M hydroquinone, by applying 0.400 V for 5 s.

Electrochemical Impedance Spectroscopy (EIS) measurements were performed with an Autolab128N at −0.100 V, between 10 kHz and 10 mHz, with ΔE = 10 mV using 5.0×10^{-2} M H_2O_2. The impedance spectra were analyzed using the Z-view program.

Electrochemical measurements were performed in deoxygenated solutions. Charge–discharge curves were recorded using a current of $1.0\ A \cdot g^{-1}$. Some samples were also electrochemically reduced ($GNR_{XXX\text{-}ER}$) by scanning the potential from 0.800 to −2.000 V at $0.100\ V \cdot s^{-1}$ (1 cycle). All measurements were performed at room temperature.

3. Results and discussion

3.1. Structural characterization

Fig. 1 shows TEM micrographs for different GNR samples. GNR_{000} (Fig. 1A) consists of long graphitized MWCNTs with good distribution of lengths and diameters, along with graphitic impurities. In GNR_{015} (Fig. 1B), it is possible to observe a heterogeneous material, containing oxidized, unopened MWCNTs, and MWCNTs with different degrees of unzipping. Large graphene sheets and anisotropic GNRs can be observed for GNR_{100}, (Fig. 1C), demonstrating that, at higher reaction times, the sample contains mostly unzipped MWCNTs, with some unopened MWCNTs. In the case of $GNR_{100\text{-}ER}$ (Fig. 1D), individual and entangled GNRs, together with large graphitic sheets, are evident.

XRD spectrum (Fig. 1E) for GNR_{000} shows a very strong peak at 26°, indicating a well-defined sp^2 structure, with large domains. As the reaction proceeds, this peak decreases, and a new peak appears at ~10°, due to the formation of oxygen moieties during the oxidation step. This peak reaches a maximum for the GNR_{100} sample, in agreement with the elemental analysis results (Table 1). The peak at 2θ = 26° is observed at all reaction times, indicating the existence of remaining MWCNTs. To estimate the quantity of remaining MWCNTs, a tentative approximation, as far as we know not previously used before, has been carried out by considering a parameter, defined by us as *graphitic fraction*

$$\text{Graphitic fraction} = \frac{A_{10}}{(A_{10} + A_{26})}$$

being A_{10} the area at 2θ = 10° and A_{26} the area at 2θ = 26°. Considering that A_{10} comes from GNRs, and A_{26} comes from the remaining MWCNTs. It is not a quantitative method, but it is a valid approach as much as A_{10} is correlated to the quantity of oxidized material and A_{26} is correlated to the quantity of remaining MWCNTs. Oxygen content, determined directly by elemental analysis (Table 1) increases with oxidation time until reaching the maximum for GNR_{100}, indicating overoxidation at GNR_{120}. The highest BET surface area (Table 1) was obtained at $GNR_{120\text{-}N2H4}$, while for the other hybrid samples the area increases, in general terms, with the oxidation time.

The Csp2 atomic percentage, as determined by C1s XPS, decreases when the oxidation degree increases (25.7% GNR_{015}, 15.8% GNR_{030}, 1.9% GNR_{120}, 22.8% $GNR_{120\text{-}N2H4}$), while carbonyl/quinone groups decrease as seen by O1s XPS (17.9% GNR_{015}, 9.0% GNR_{030}, 0.0% GNR_{120}, 24.2% $GNR_{120\text{-}N2H4}$). On the other hand, carboxylic groups increase with the oxidation degree (3.8% GNR_{015} and GNR_{030}, 63.8% GNR_{120}, 18.1% $GNR_{120\text{-}N2H4}$). GNR_{015} has the highest content of Csp2 and carbonyl/quinone groups and the lowest content of carboxylic groups.

The chemical reduction of GNR120 restores part of the C-sp2 structure and carbonyl/quinone groups and decreases the electrically insulating carboxylic group content that does not reach the low content determined for GNR_{015} sample. SEM micrographs of deposited electrodes show a higher stacking of layers for $GNR_{120\text{-}N2H4}$ (Fig. 1G) than for GNR_{015} (Fig. 1F).

3.2. Electrochemical characterization

The highest capacity, determined by galvanostatic experiments, was obtained for GNR_{015}, followed by reduced materials (Table 1). The highest electroactive areas were also obtained for GNR_{015} (Table 1). CVs in supporting electrolyte (not shown) follow the same trend as capacity and electroactive area measurements. Although higher BET areas should lead to higher capacities and electroactive areas, there is a considerable stacking in $GNR_{120\text{-}N2H4}$ sample observed by FE-SEM. Furthermore, the content of conductive Csp2, oxygen, and electroactive carbonyl-quinone groups in GNR_{015}, results in a higher capacity and electroactive area.

To evaluate if the electrochemical response of the materials is only due to their electroactive area or there is also an improvement in charge transfer, amperometric experiments were performed using H_2O_2 as redox marker. A sensitive and fast amperometric response was obtained at −0.100 V for successive additions of 5.0×10^{-4} M H_2O_2. Fig. 2A shows the calibration plots for the different modified GCEs. The highest sensitivity was obtained for GCE/GNR_{015}, $(0.85 \pm 0.07)\ \mu A \cdot mM^{-1}$. The sensitivity reaches a value 87 times higher than the one obtained for GCE/GNR_{000}, 3 times higher than the one obtained for GCE/$GNR_{120\text{-}N2H4}$ and 4 times higher than the one obtained for GCE/$GNR_{120\text{-}ER}$, demonstrating the advantages of this sample on the reduction of H_2O_2. The extremely low activity observed for GCE/GNR_{000} discards the presence of electrocatalytic metals on the starting material [15,16]. GCE/GNR_{015} presents the best compromise between unzipped MWCNTs, C-sp2 and electrochemically active carbonyl/quinone groups, thus showing the best electrochemical performance.

For better comprehension of its electrochemical behavior, the system was evaluated by EIS (Fig. 2B). The model proposed considers that the surface consists of different regions, covered and uncovered, which can act in parallel. Electron transfer occurs on the covered regions as well as on the macroscopic uncovered zones. In the equivalent circuit (Fig. 2B) the electrolyte resistance (R_s) is in series with the charge transfer resistance (R_{ct}), which is in parallel with the double layer

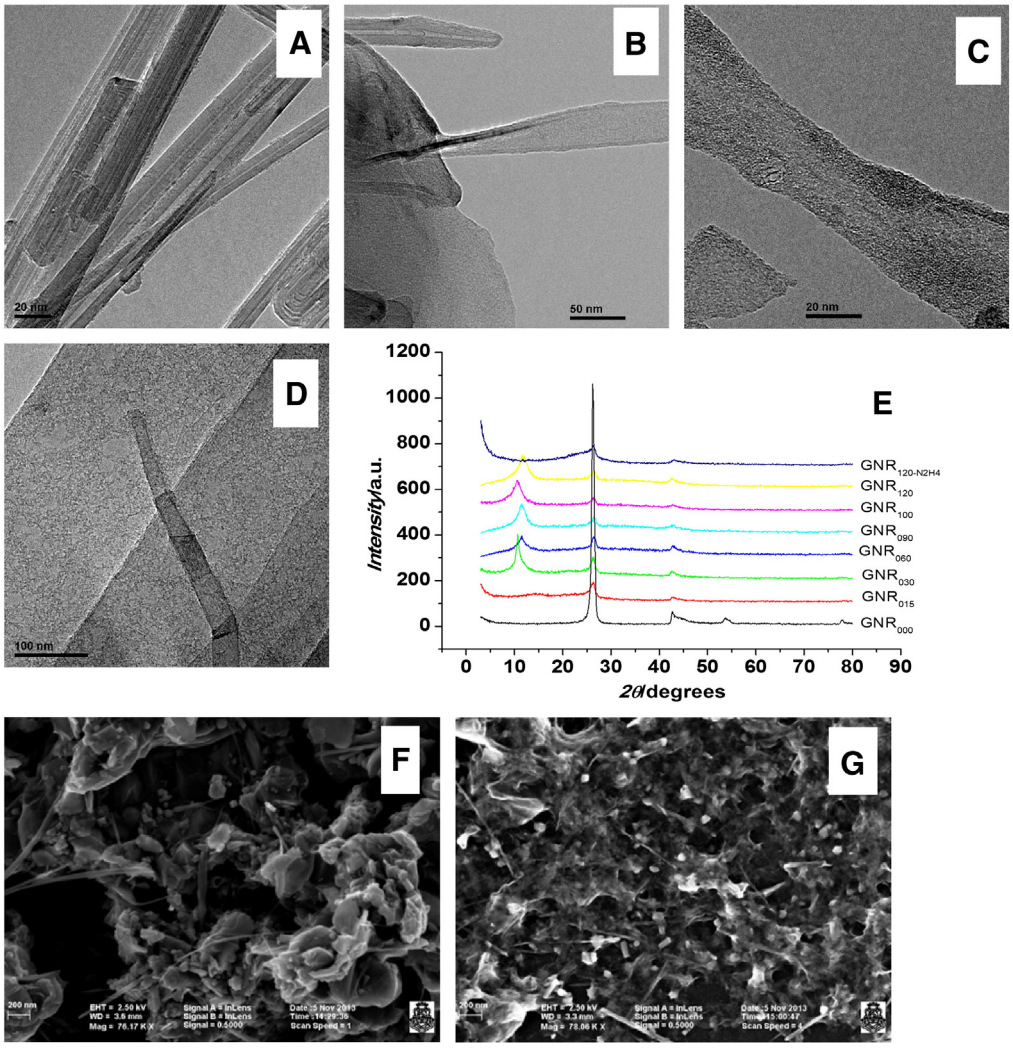

Fig. 1. Physical characterization of the obtained materials. From A to D, TEM micrographs for GNR_{000}, GNR_{015}, GNR_{100} and $GNE_{100\text{-}ER}$, respectively. E) XRD spectra for the materials synthesized in this work. F and G, FE-SEM images of the GNR_{015} and $GNR_{120\text{-}N2H4}$ modified electrodes, respectively.

capacitance (C_{dl}). The circuit includes two additional elements, a $C_{dl\text{-}uc}$ and a $R_{ct\text{-}uc}$ associated with the uncovered zones. Fig. 2C shows a plot for the charge transfer resistance as a function of the different surfaces. As Table 1 shows, GCE/GNR_{015} presents the lowest value of R_{ct}. These results allow concluding that GCE/GNR_{015} provides a more efficient electron transfer towards H_2O_2 reduction, in agreement with the sensitivity observed in the amperometric experiments.

Analytical parameters for the reduction of H_2O_2 (sensitivity, detection limit (LOD), linear range) at the different modified GCEs are summarized in Table 1. In general, higher sensitivity and lower R_{ct} are obtained for GCE/GNR_{015}, not only due to its high electroactive area but also to their better reactivity, since when the sensitivity and R_{ct} are normalized to this area, GCE/GNR_{015} presents important differences compared to the other samples.

The comparison with other graphene materials indicates that our sensor presents better LOD than [17–19]. The detection limits of [20–22] are better than the ones reported in this work, although our sensor presents the advantage of using a very simple transduction scheme and electrode preparation compared to them (LOD taken as 3.3 × standard deviation of the blank signal/sensitivity). From this

Table 1
Oxygen content, BET area, graphitic fraction, electrochemical parameters and analytical parameters for the amperometric determinations of H_2O_2 for the different materials synthesized in this work.

Material	%O (direct determination)	BET area/$m^2 \cdot g^{-1}$	Graphitic fraction	Positive charge capacity (F/g)	Electroactive area/cm^2	R_{ct}/Ω	Sensitivity/$\mu A \cdot mM^{-1}$	LOD/μM	Linear range/mM
GNR_{000}	0.49	30	1.00	6.6	$(7 \pm 1)10^{-3}$	222,500	$(1.0 \pm 0.1)10^{-2}$	146.0	0.5–2.5
GNR_{015}	22.09	54	0.48	84.1	$(1.0 \pm 0.1)10^{-2}$	9777	0.85 ± 0.07	1.7	0.5–3.0
GNR_{030}	32.88	60	0.32	37.4	$(5100 \pm 6)10^{-6}$	21,228	$(120 \pm 3)10^{-3}$	12.0	0.5–2.5
GNR_{060}	36.65	78	0.41	35.6	$(5 \pm 1)10^{-3}$	35,044	0.16 ± 0.01	9.0	0.5–2.5
GNR_{090}	41.93	130	0.30	20.8	$(6.0 \pm 0.3)10^{-3}$	74,453	$(20 \pm 0.2)10^{-3}$	72.2	0.5–2.0
GNR_{100}	43.39	102	0.18	19.8	$(6.7 \pm 0.5)10^{-3}$	342,132	$(22 \pm 4)10^{-3}$	65.7	0.5–2.5
GNR_{120}	40.49	161	0.28	23.1	$(5.8 \pm 0.8)10^{-3}$	237,672	$(32 \pm 5)10^{-3}$	45.0	0.5–3.0
$GNR_{120\text{-}ER}$	N/A	N/A	N/A	79.8	$(6.5 \pm 0.8)10^{-3}$	68,932	0.22 ± 0.01	6.6	0.5–3.5
$GNR_{120\text{-}N2H4}$	14.00	185	N/A	64.5	$(9 \pm 3)10^{-3}$	55,059	0.28 ± 0.08	5.2	0.5–3.0

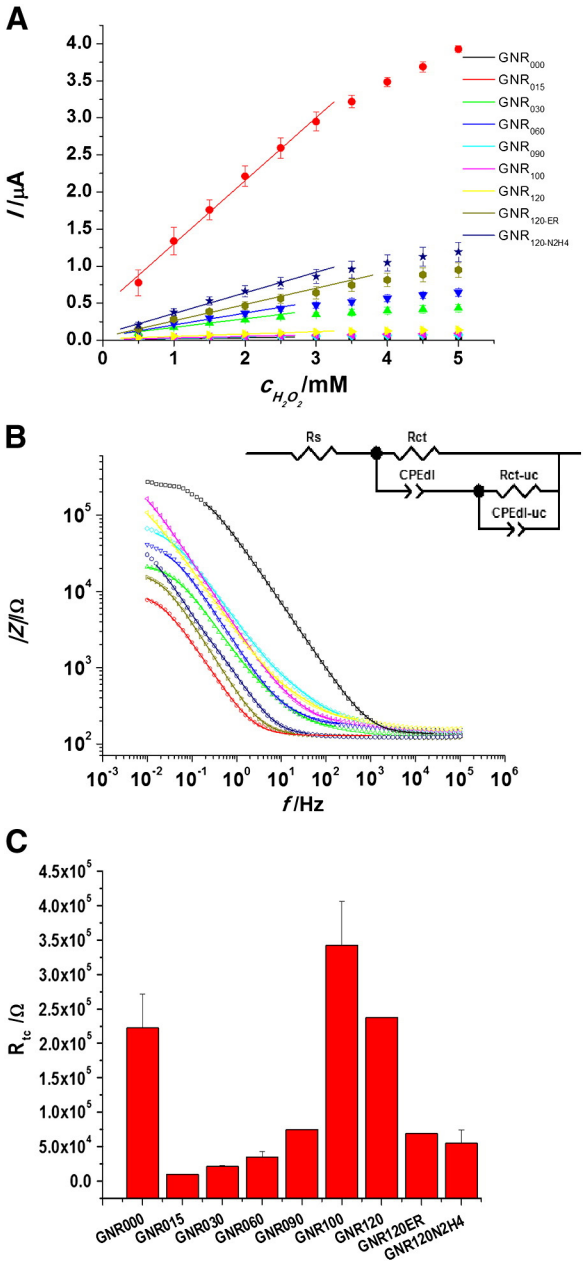

Fig. 2. Electrochemical characterization of the obtained materials, A) Calibration plots obtained from amperometric experiments at GCEs modified with the different nanomaterials for consecutives additions of H_2O_2. B) Bode plot for the modified GCEs with the different nanomaterials: experimental data (dots) and fitting to the proposed model (line) C) Charge transfer resistance (R_{tc}) for the GCEs modified with the different nanomaterials:.

comparison, it is important to mention that the response obtained here is more sensitive than that reported in [18,23] using nanoparticles supported on graphene. The electrochemical properties of GNR_{015}, due to the combined effects of electrochemically accessible area, the content of Csp2, the high content of electrochemically active carbonyl/quinones groups and the low content of insulating carboxylic groups, represent a new avenue for improving the performance of electrochemical (bio)sensors based on the detection of H_2O_2 and other analytes.

Electron transfer kinetics was studied using CV following the procedure described in 2.4. GCE/GNR_{000} showed the lowest k^0 (0.0032 $cm \cdot s^{-1}$) as a consequence of the highly graphitized, defect-free structure of arc-discharge MWCNTs. Literature assumes that the CNT side wall is inert and that open ends and defect sites are responsible for the observed electron transfer activity [9,24]. Exfoliated homogeneous materials with oxygen groups, ($88 > \Delta E_p > 83$ mV), present higher electron transfer rate, but within the same magnitude order (GNR_{120} 0.0079 $cm \cdot s^{-1}$, $GNR_{120\text{-}ER}$ 0.0086 $cm \cdot s^{-1}$, $GNR_{120\text{-}N2H4}$ 0.0097 $cm \cdot s^{-1}$), similar to those obtained for a single-layer graphene electrode [25]. GCE/GNR_{015} showed $\Delta E_p = 61$ mV, indicating a nearly reversible reaction, and a k^0 of 0.11 $cm \cdot s^{-1}$, ten times higher than for homogeneous oxygenated materials.

4. Conclusions

The results presented here demonstrate that by controlling the reaction time and using a low-cost and relatively simple experimental setup, we have been able to synthesize a hybrid GNR-MWCNT material that presents the highest electroactive area, the faster electron transfer and the highest sensitivity towards H_2O_2 reduction. GNR_{015} presents the best compromise between unzipped MWCNTs, C_{sp2} content and electrochemically active oxygenated functional groups, showing the best electrochemical performance. The higher amount of carbonyl-quinone groups and C_{sp2} content, and the lower amount of carboxylic groups of GNR_{015} sample are responsible for the superior electrochemical performance compared to the chemically reduced sample. This material represents a promising support in very important electrochemical fields such as sensing, biosensing, supercapacitors and electrocatalysis.

Acknowledgments

This work was funded by Spanish MINECO, projects TEC2010-15736 and PRI-PIBAR-2011-1, and Argentinean MINCyT, project PICT MICINN 2011–2748.

References

[1] A.L. Higginbotham, D.V. Kosynkin, A. Sinitskii, Z. Sun, J.M. Tour, ACS Nano 4 (2010) 2059.
[2] D.V. Kosynkin, A.L. Higginbotham, A. Sinitskii, J.R. Lomeda, A. Dimiev, B.K. Price, J.M. Tour, Nature 458 (2009) 872.
[3] M. Pumera, Chem. Soc. Rev. 39 (2010) 4146.
[4] M. Pumera, Chem. Eur. J. 15 (2009) 4970.
[5] B. Šljukić, C.E. Banks, R.G. Compton, Nano Lett. 6 (2006) 1556.
[6] M.S. Goh, M. Pumera, Electrochem. Commun. 12 (2010) 1375.
[7] A. Martin, J. Hernandez, L. Vazquez, M.T. Martinez, A. Escarpa, RSC Adv. 4 (2014) 132.
[8] F. Valentini, M. Carbone, G. Palleschi, Anal. Bioanal. Chem. 405 (2013) 3449.
[9] C.-L. Sun, C.-T. Chang, H.-H. Lee, J. Zhou, J. Wang, T.-K. Sham, W.-F. Pong, ACS Nano 5 (2010) 7788.
[10] W. Grosse, J. Champavert, S. Gambhir, G.G. Wallace, S.E. Moulton, Carbon 61 (2013) 467.
[11] L. Buglione, M. Pumera, Electrochem. Commun. 17 (2012) 45.
[12] A.M. Benito, W.K. Maser, M.T. Martínez, Int. J. Nanotechnol. 2 (2005) 71.
[13] R.S. Nicholson, Anal. Chem. 37 (1965) 1351.
[14] F.C. Anson, R.A. Osteryoung, J. Chem. Educ. 60 (1983) 293.
[15] M. Pumera, A. Ambrosi, E.L.K. Chng, Chem. Sci. 3 (2012) 3347.
[16] C.H.A. Wong, C.K. Chua, B. Khezri, R.D. Webster, M. Pumera, Angew. Chem. Int. Ed. 52 (2013) 8685.
[17] W. Lu, Y. Luo, G. Chang, X. Sun, Biosens. Bioelectron. 26 (2011) 4791.
[18] Y. Ye, T. Kong, X. Yu, Y. Wu, K. Zhang, X. Wang, Talanta 89 (2012) 417.
[19] X. Liu, H. Zhu, X. Yang, Talanta 87 (2011) 243.
[20] M. Zhou, Y. Zhai, S. Dong, Anal. Chem. 81 (2009) 5603.
[21] H. Teymourian, A. Salimi, S. Khezrian, Biosens. Bioelectron. 49 (2013) 1.
[22] L. Li, Z. Du, S. Liu, Q. Hao, Y. Wang, Q. Li, T. Wang, Talanta 82 (2010) 1637.
[23] Y. Zhang, X. Sun, L. Zhu, H. Shen, N. Jia, Electrochim. Acta 56 (2010) 1239.
[24] A. Holloway, G. Wildgoose, R. Compton, L. Shao, M.H. Green, J. Solid State Electrochem. 12 (2008) 1337.
[25] N.L. Ritzert, J. Rodríguez-López, C. Tan, H.D. Abruña, Langmuir 29 (2013) 1683.